JOURNAL OF SPACECRAFT AND ROCKETS
Vol. 46, No. 2, March–April 2009

Deployment Analysis of Lenticular Jointed Antennas Onboard the Mars Express Spacecraft

Mehran Mobrem*
Northrop Grumman Space Technology Astro Aerospace, Carpinteria, California 93013
and
Douglas S. Adams†
Jet Propulsion Laboratory, California Institute of Technology, Pasadena, California 91109

DOI: 10.2514/1.36890

Extensive analytical and experimental activities were carried out that culminated in successful deployments in May and June of 2005 of three lenticular, jointed booms that formed a first of its kind of ground penetrating radar antenna onboard the Mars Express spacecraft. These activities went well beyond the normal required tasks due to a postlaunch realization that the stowed booms retained a high level of stored energy. This high level of stored energy resulted in an uncontrolled boom deployment rather than a predictable boom deployment. Experimentally measured straight section properties and hinge properties were incorporated into specialized modeling techniques that were then used to simulate the boom lenticular joints. System level models were exercised to understand the boom deployment dynamics and spacecraft level implications including spacecraft attitude control and possible entanglement. Discussion includes a comparison of deployment simulation results to measured flight data taken during the three boom deployments. Important parameters that govern lenticular joint behavior are outlined and a short summary of lessons learned and recommendations is included to better understand future applications of this technology.

Nomenclature

$[C]$	=	Rayleigh damping matrix
f	=	frequency, Hz
$\{f_d\}$	=	damping force vector
I_{yy}	=	spacecraft mass moment of inertia, kg · m^2
$[K]$	=	structural stiffness matrix
$[M]$	=	structural mass matrix
T_g	=	glass transition temperature, °C
t	=	time, s
$\{V\}$	=	component velocity vector
$\{Y\}$	=	component displacement vector
α	=	mass proportional damping constant
β	=	stiffness proportional damping constant
ε	=	structural damping
ζ_i	=	ith modal damping
ω_i	=	ith modal frequency, rad/s
ω_y	=	spacecraft angular velocity, rad/s

I. Introduction

THE Mars Advanced Radar for Subsurface and Ionospheric Sounding (MARSIS) antenna is part of an instrument payload onboard ESA's Mars Express spacecraft which launched on 2 June 2003, and entered Mars orbit on 25 December 2003. MARSIS is a long wavelength radar sounder that will be used to perform measurements on the Martian ionosphere and to search for evidence of subsurface water. It is designed to operate at altitudes up to 800 km above the Martian surface for subsurface sounding, up to 1200 km for ionospheric sounding, and is capable of making measurements in 1 MHz wide bands centered at 1.8, 3.0, 4.0, and 5.0 MHz. This flexible design allows MARSIS to search for evidence of water as deep as 5 km below the surface.

The antenna for the MARSIS experiment was developed and built by Northrop Grumman Space Technology (NGST) Astro Aerospace. The antenna is made of three foldable, flattenable tubes (FFT)™. A full description of the design is presented in [1]. The FFT is an ultralightweight deployable structure that is designed purely for use in a space environment. As such, any significant friction, gravity, or air drag, combined with its large dimensions, renders terrestrial based testing of the FFT intractable. Therefore, the verification process for the FFT deployment relied solely on component level testing and analytical simulations performed using Automatic Dynamic Analysis of Mechanical Systems (ADAMS) software.

The original deployment simulation of the MARSIS antenna, done in 2000, underestimated its dynamics due to misleading documentation of damping in ADAMS and an overestimate of the hinge strength. The typical damping implementation in software used for dynamic analysis, such as ADAMS or Dynamic Analysis and Design System (DADS), does not work properly for time-variant structures such as the FFT. The correct application of damping for time-variant structures should be the implementation of structural or hysteretic damping. In early 2004, during the design and analysis of a much shorter FFT for the shallow radar antenna, it was discovered that the term "structural damping" in the ADAMS manual is used incorrectly to describe a Rayleigh damping implementation. As a result of this error, the ADAMS model of the MARSIS antenna had unrealistic modal damping that varied from 188% to 1% during the deployment instead of a constant 1% as intended. This artificially high damping resulted in benign behavior during the original deployment analysis which did not show any significant dynamics. However, after correcting for the application of damping in 2004, the new deployment analysis showed significant dynamics in which the FFT hinges would undergo multiple buckling events during the deployment. This resulted in a highly dynamic and chaotic behavior. This information was immediately communicated to both the Jet Propulsion Laboratory and ESA.

Presented as Paper 1683 at the 47th AIAA/ASME/ASCE/AHS/ASC Structures, Structural Dynamics, and Materials Conference, Newport, Rhode Island, 1–4 May 2006; received 28 January 2008; revision received 18 August 2008; accepted for publication 21 September 2008.

*Chief Analyst, Engineering, 6384 Via Real. Member AIAA.
†Senior Engineer, Spacecraft Structures and Dynamics Group, 4800 Oak Grove Drive. Member AIAA.

The deployment of MARSIS, which was initially scheduled for 20 April 2004, was delayed after the discovery that the original analysis had underestimated the deployment dynamics. Over the course of the following year an intense analysis and testing effort was undertaken that focused on more accurately quantifying the deployment, validating the ADAMS model, and assessing any risk to the health of the Mars Express spacecraft. Component testing went beyond the original tests done in order to characterize the postbuckling behavior of the hinges and their residual strength capability after multiple buckling events. This was necessary because repeated buckling was anticipated based on the increased dynamics in the updated model. The FFT is not designed to take any significant buckling during the deployment and, if the excess dynamics had been known at that time, the MARSIS design would have been modified to reduce its stowed energy. Component test results were incorporated into an updated ADAMS model of the deployment which included an automated damping algorithm to account for the discontinuous boom lengths encountered during the deployment. This model was then exercised in a Monte Carlo study to determine the probability of a successful or dangerous deployment outcome.

MARSIS employs a total of three FFT booms with two that form a 40 m dipole and the third acting as a 7-m monopole antenna. The booms have periodic slotted hinge sections where some material is removed which then allows the Kevlar® and fiberglass composite tubes to be folded elastically without permanent deformation. The folded booms are then compressed accordion style into a cradle for launch and the journey to Mars as shown in Fig. 1. Each boom is thus a single piece structure in its deployed state with all joints fastened and bonded before launch. The deployed dipole and monopole antenna configuration is illustrated along with the Mars Express spacecraft in Fig. 2. The actual antenna is a pair of 22 gage wires that run the length of the interior in all three booms.

Although the operation of a single lenticular (carpenter tape) hinge is straightforward in a shirt sleeve environment, the simultaneous deployment of multiple hinges in a space environment has proven to be a challenging problem. Environmental effects, combined with uncertainty in the dynamics, make it impossible to deterministically evaluate the flight behavior of the deployment. The MARSIS mechanical team was faced with the daunting task of quantifying the potential boom dynamic behavior and determining the corresponding risk to the spacecraft given only limited knowledge of the boom properties (postbuckling) on station. The pre- and postdeployment analysis proved formidable and brought to light the uncertain nature inherent to the deployment of serially linked lenticular hinges. As mentioned previously, one of the key issues with a large deformation deployment such as MARSIS is that friction, gravity, and aerodynamic resistance forces dominate terrestrial testing. The boom is extremely lightweight and its properties are also temperature dependent. As a result of the influence of these forces it is impossible to test the full system behavior before flight and the analysis must be relied upon to predict the deployment dynamics.

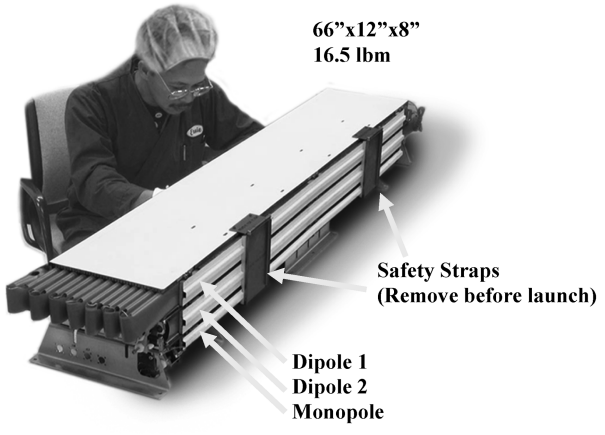

Fig. 1 Stowed MARSIS antenna FFT booms and cradle before launch.

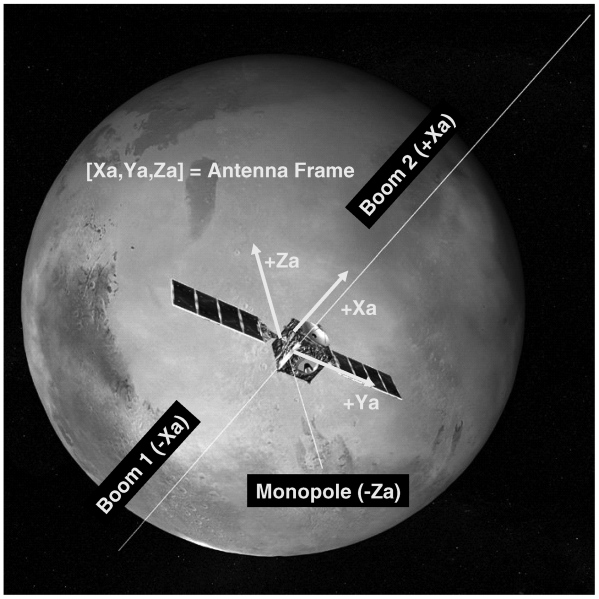

Fig. 2 The three deployed MARSIS booms and the reference antenna coordinate system.

II. Analysis Approach and Validation

ADAMS software was used as the primary analysis tool and a highly specialized ADAMS model was used to simulate all three of the MARSIS boom deployments. The model was constructed with 13 straight segments connected by spline hinge joints that reproduced the measured hinge torque profile, buckling strengths, and postbuckling behavior. Each of the 13 straight segments was composed of two beam elements that employed an automated algorithm to update the damping factor parameter based on the local straight section beam length and the corresponding end conditions. Note, in ADAMS, the term structural damping is used for stiffness proportional Rayleigh damping, which was still used but in a highly modified and discontinuous fashion. Finally, the accordion style stowed state was modeled with gap springs connecting adjacent boom segments in order to capture the stowed compressive energy. The schematic of the dipole boom system is presented in Fig. 3.

A. Damping Implementation

The damping force $\{f_d\}$ due to Rayleigh or proportional damping $[C]$ is given by [2]

$$\{f_d\} = [C]\{V\} \tag{1}$$

where $\{V\}$ is the component velocity vector and

$$[C] = \alpha[M] + \beta[K] \tag{2}$$

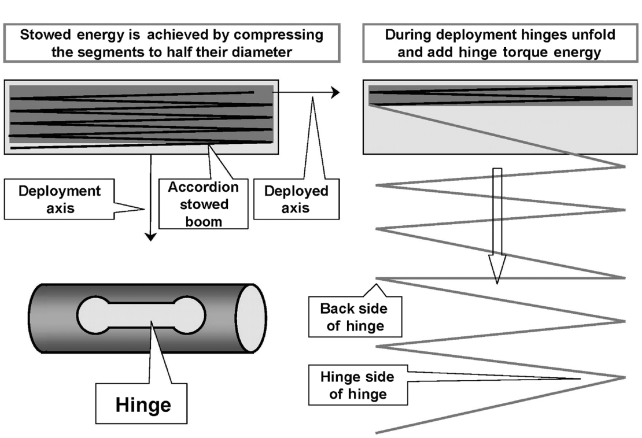

Fig. 3 Dipole construction, stowage, and deployment process.

where $[M]$ is the mass matrix, $[K]$ is the stiffness matrix, and α and β are the mass and stiffness proportional constants, respectively. In ADAMS, only the stiffness proportional damping constant β is used and is termed the structural damping factor. The modal damping ζ_i for the ith mode is given by

$$\zeta_i = 0.5\beta\omega_i \tag{3}$$

where ω_i is the natural frequency of the ith mode.

The use of proportional damping is acceptable for time-invariant structures where the damping factor β is selected based on the modal damping of the structure's fundamental mode. When this is done, a higher modal damping will be observed at the higher modes which somewhat represents the behavior of real structures. However, in time-variant structures such as the MARSIS booms, the use of a single Rayleigh damping value is not acceptable because the modal damping for the fundamental mode should always be the same regardless of its natural frequency value.

In the case of the MARSIS antenna, the natural frequency of the first two segments at the tip after their connecting hinge becomes fully locked is about 15 Hz; for a modal damping of 1% the damping factor β should be 0.0002. In the other extreme, the natural frequency of the fully deployed antenna is about 0.08 Hz; in this case, the damping factor β should be 0.04 to achieve 1% modal damping. The same damping factor β used for the fully deployed antenna would result in unrealistic modal damping of 188% if applied for the two straight segments.

An automated routine was written and implemented as a user defined beam element in the ADAMS software to mitigate this issue. The routine updates the damping factor β for each individual segment after a hinge changes state (either unlocked to locked or locked to unlocked) and the local straight section (composed of 1 to 13 segments) takes on a different natural frequency. Four different configurations were selected to compute the straight section's fundamental natural frequency: pinned–free for the tip section, pinned–pinned for the interior section, and both fixed–pinned and fixed–free for the root section. At each time step the program would examine the current configuration and determine the state of each hinge. Then, using these hinge states, the program would assign an appropriate β for each segment based on the length and boundary conditions of its parent straight section. This approach is somewhat nonconservative because the damping factor β is computed assuming each segment would vibrate at its fundamental mode and during the ADAMS simulation it was observed that some segments did vibrate at higher modes (e.g., immediately after a hinge locks or unlocks).

In a separate effort a different approach was used to solve this problem by using a true structural damping model. A version of structural damping was incorporated into the ADAMS software and used to validate the first approach. However, the actual time to run a single problem was over 30 h which made the solution prohibitively slow. The damping force $\{f_d\}$ due to structural or hysteretic damping ε is given by [3]

$$\{f_d\} = \varepsilon[K]\{|Y|\text{sign}(V)\} \tag{4}$$

where $\{Y\}$ is the component displacement vector and the relation between modal damping ζ and structural damping is given by $\varepsilon = \pi\zeta$.

B. Model Verification

Because a ground based full system deployment test for the MARSIS booms was not possible, relying on analysis was the only means available to determine its on-orbit deployment characteristics. Therefore, validation of the ADAMS model was critical to substantiate any resulting conclusions. The validation process was accomplished through component static testing combined with simplified dynamic testing. Test results are described in the next section.

In addition, a second model was commissioned using ABAQUS software to gain more insight into the hinge behavior both in quasi-static and dynamics environments. The deployment from the stowed configuration of a two segment antenna, connected with a midhinge, was evaluated in the ABAQUS analysis as shown in Fig. 4. In the quasi-static mode the ABAQUS model deployment was used to characterize the hinge deployment torque, buckling capability, and postbuckling behavior. A typical torque profile from this analysis is presented in Fig. 5 and the associated buckling strength is presented in Fig. 6. The predicted hinge stiffness in Figs. 5 and 6 is similar to published analytical and finite element results [4,5] although the primary modeling objective was to explore the buckling mechanisms. In the dynamic mode the stowed constraint was removed suddenly simulating the opening of the cradle door allowing the dynamic deployment of the segments. The purpose of this analysis was to evaluate the buckling capability of the hinge under dynamic loading. It was concluded that the bucking capability of the hinge is similar for both the static and dynamic environments.

Finally, a third model was also commissioned using DADS software to help verify the ADAMS computational (numerical) routine by creating two similar models in ADAMS and DADS. Note

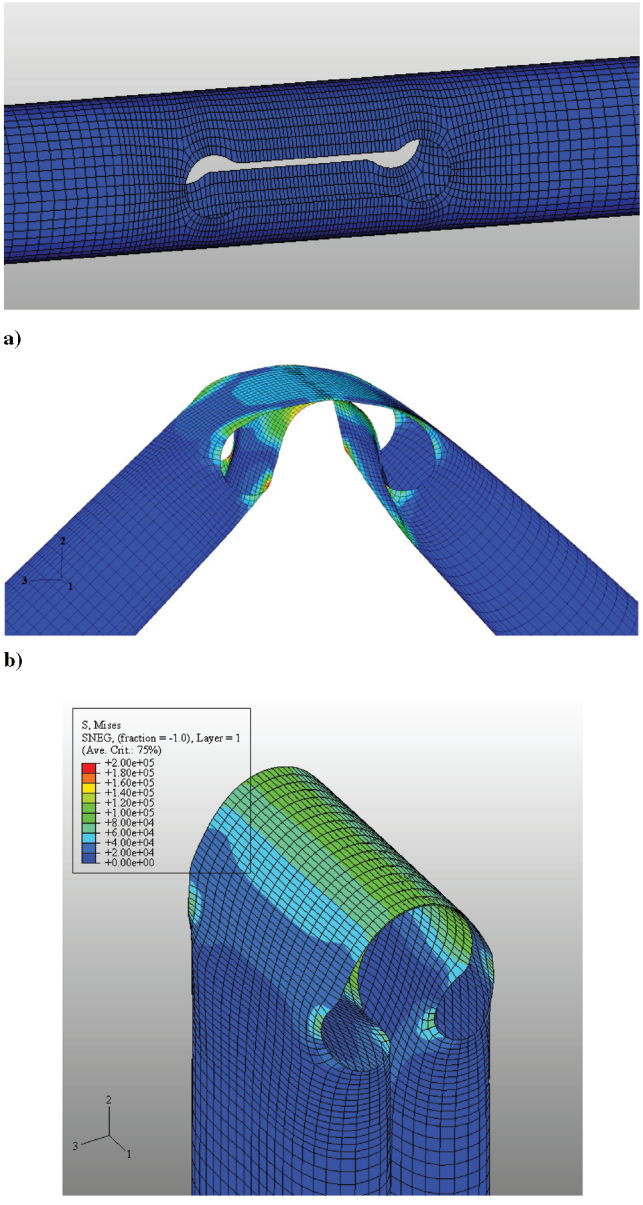

Fig. 4 a) Undeformed FFT hinge area mesh modeled in ABAQUS; b) hinge area of FFT partially folded with a 90 deg angle between the straight segments; and c) hinge area of FFT after folding to a 180 deg angle and compressing the diameter by 50%.

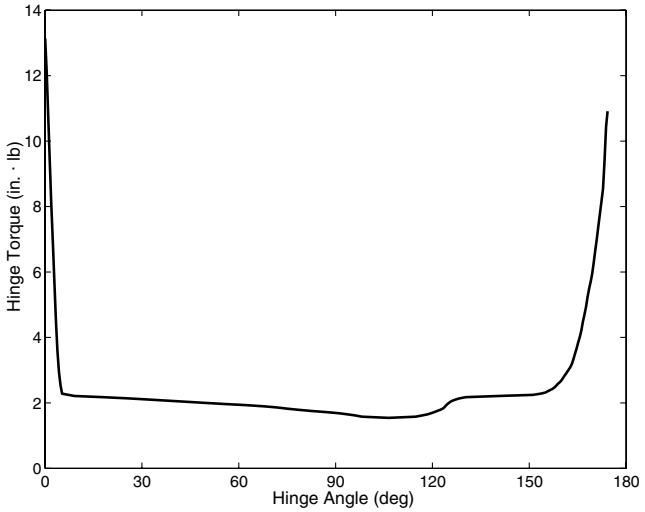

Fig. 5 ABAQUS hinge model torque vs hinge angle during quasi-static unfolding.

the implementation of damping in DADS (component modal damping) would result in a similar erroneous result for time-variant structures. Therefore, these models were limited in size with most having one or two hinges. The ADAMS and DADS results were found to be consistent with each other.

C. Component Testing

Because of the infeasibility of a full system test a computational study was used to determine the critical controlling parameters of the deployment. This resulted in narrowing the planned component testing to three major parameters: the hinge buckling strength, the hinge torque profile, and the stowed compressive energy.

1. Hinge Buckling Strength

The hinge buckling strength was measured using sections of the flight spare booms in a four-point bending fixture. The spare booms were from a qualification unit and were kept in the stowed configuration from the time of launch. Results from this test indicated that the in situ hinge strength was lower than previous measurements mainly due to thermal environment and aging. Also the hinge buckling could occur both in and adjacent to the hinge section. The mechanism for buckling in the vicinity of the hinge section is illustrated by the ABAQUS results shown in Fig. 7. There was a reduction in hinge buckling strength after a buckling and

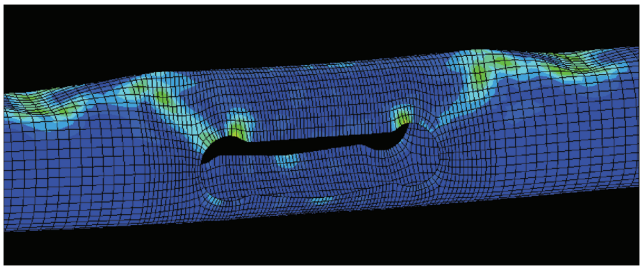

Fig. 7 ABAQUS dynamic simulation results showing buckling of the straight tube section at locations outside of the slotted hinge area.

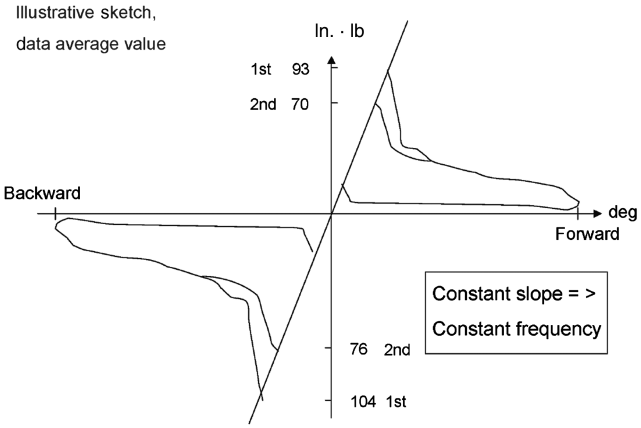

Fig. 8 Hinge model for buckling and postbuckling torque used in ADAMS.

postbuckling cycle due to some fiber failure and localized matrix damage. However, after many buckling cycles, the hinges were still able to deploy and become fully locked with minimal stiffness reduction and their residual strength was adequate for on-orbit operation. A typical buckling and postbuckling behavior of the hinge used in the ADAMS analysis is presented in Fig. 8.

2. Hinge Torque

The hinge torque was measured both at room temperature and in an environmental chamber at its on-orbit temperature of −70°C to better characterize its contribution to the deployment energy as well as the hysteresis energy dissipation associated with hinge buckling and postbuckling events. The hinge torque measured at room temperature for a typical hinge is shown in Fig. 9 which has a similar

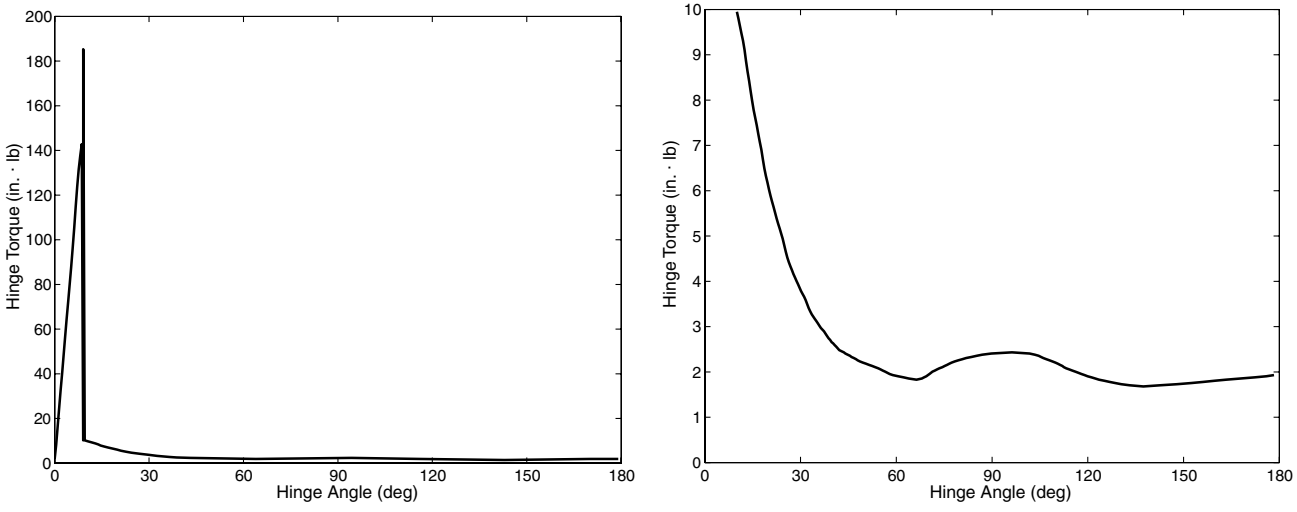

a) **b)**

Fig. 6 a) ABAQUS hinge model buckling torque vs hinge angle; b) ABAQUS hinge model postbuckling torque vs hinge angle.

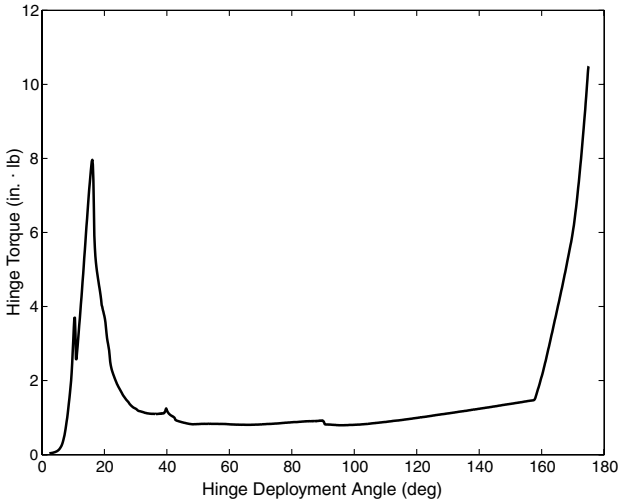

Fig. 9 Typical measured hinge deployment torque profile at room temperature.

torque profile to the ABAQUS computational prediction shown in Fig. 5. Note that the test sample has seen many deployment cycles, has gone through qualification testing including the thermal cycles, and has been in stowed configuration since before launch in 2003. As a result of this a significant reduction in deployment torque has been observed compared to a pristine hinge.

A plausible explanation for torque reduction is the viscoelastic flow of the matrix relative to the fibers in the composite material. It should be noted that the stowed hinges are highly stressed and, as a result, the material will creep especially at higher temperature. The hinges are stowed at room temperature and when they are held in this configuration for a long time and have gone through multiple thermal cycles, then it is possible that the hinges will take a set to a new configuration and consequently lose some of their stowed energy. This phenomenon is much more noticeable when the hinges are deployed at cold temperature where the matrix becomes stiffer and it is more difficult for the fibers to overcome the new condition of the (frozen) matrix. The average hinge torque profile used in the ADAMS dynamic simulation corresponds to −70°C and is shown later in Fig. 11; note the negative torque region in Fig. 11 near a hinge angle of 50 deg which represents a secondary stability point and is associated with "freezing" or "stalling" of the hinge.

3. Stowed Energy

In a third series of tests the stowed energy due to the compression of the tube diameter in the cradle was measured in a vacuum chamber at −70°C and found to be 215 in. · lb for the two dipole booms and 38 in. · lb for the monopole boom.

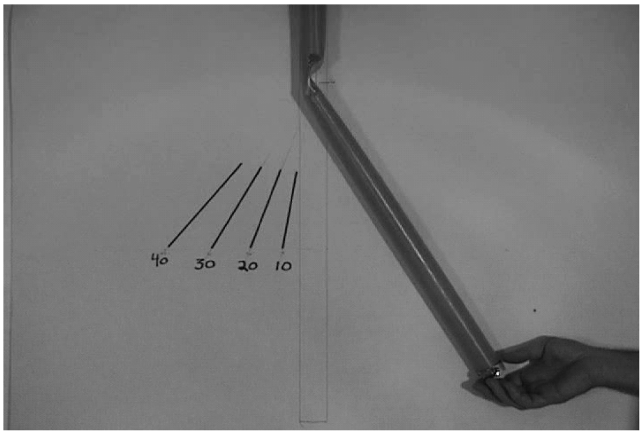

Fig. 10 Vertical pendulum test to validate the ADAMS hinge model implementation.

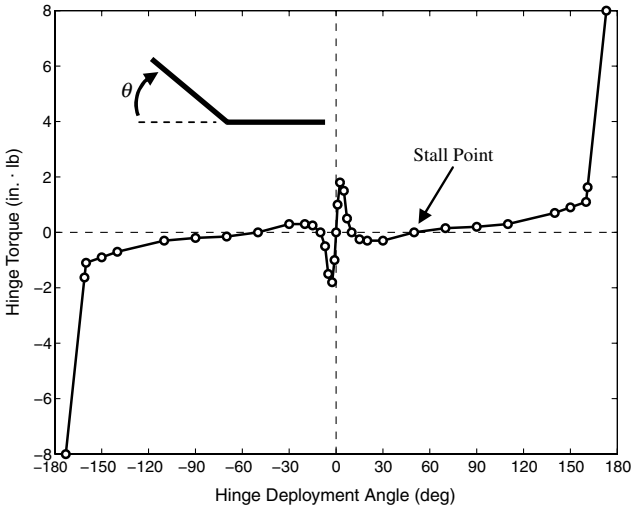

Fig. 11 Average hinge deployment torque profile at −70°C. Note the onset of negative torque at ∼50 deg that can lead to a stall condition for low angular rates. The artificially steep slope near 180 deg is intended to prevent hinge self-penetration.

4. Natural Frequency and Modal Damping

A 10 m segment of antenna (half of the 20 m flight length) was used to validate the antenna finite element model and determine its modal damping. The antenna segment was tested in a vertical cantilevered configuration by releasing the tip from a deflected position and measuring the decaying tip motion. Determination of modal damping was done by simulating the test configuration in ADAMS which included the effects of gravity and air drag.

5. Vertical Pendulum Test

A single hinge in a vertical pendulum configuration was used to validate the ADAMS hinge model as it buckles dynamically. The test setup is presented in Fig. 10. The hinge properties were determined through static load tests and then incorporated into a representative ADAMS model. There was excellent correlation between the test results and the ADAMS simulation (both air resistance and gravity were considered in the analysis).

D. Inputs to the ADAMS Model

A comparison of the critical properties of the MARSIS antenna based on component testing is presented in Table 1. The antenna properties used in the Monte Carlo simulation are presented in Table 2 and Figs. 11 and 12. The residual buckling capability of each hinge after its first buckling was estimated as 75% of the initial value.

E. Analysis Results

A total of 1000 cases of the ADAMS model were run in a Monte Carlo study of the deployment dynamics. One of the key results from the Monte Carlo analysis was the discovery that a

Table 1 Comparison of critical ADAMS model parameters

Critical parameter list	Prelaunch	April & May 2004	Final
Modal damping, %	∼188[a]	3.5	3.5
Stowed energy, in. · lb	350	280	215
Hinge deploy energy, in. · lb	∼3.0	∼3.0	1.5
Hinge buckling torque, in. · lb	120/160[b]	120	104/93[c]
Hinge postbuckling hysteresis, in. · lb	∼2.0	∼2.0	7.5/5.7[c]

[a]The high original damping parameters resulted from incorrect ADAMS software modeling documentation.
[b]The hinge buckling used in the pre-2000 analysis is 120 in. · lb. After the excess dynamics was discovered one brand new spare sample was tested to 160 in. · lb.
[c]The high values are for the direction opposite of stow (A side) and the low values are in the direction of stow (B side).

Table 2 Parameters varied in the Monte Carlo analysis

Variable	Nominal	Range	Distribution	Description
ζ_1	3.5%	2–5%	Gaussian	Beam modal damping
SFACTOR	0.6	0.4–0.8	Uniform	Hinge spline scaling factor (used to vary the hinge torque profile & energy)
ENERGY	215	205–225	Uniform	Stored compressive energy, in. · lb
ABUCKLE	104	78–130	Uniform	A-side or backbuckling direction hinge strength, in. · lb
BBUCKLE	0.9	0.8–1.0	Uniform	B-side or hinge direction strength as a fraction of the A-side strength
PBM1	36.8	18.4–55.2	Uniform	Postbuckling moment 1, in. · lb
PBM2	10.0	5–15	Uniform	Postbuckling moment 2 scaled using the same fraction of nominal as 1, in. · lb

number of scenarios were possible that could result in the boom recontacting the spacecraft during the deployment. Because of the high level of stowed compressive energy the dipole boom reaches its full 20 m length in about 2.5 s, after which it typically experiences a "bullwhip"-type behavior and tends to fold back toward the spacecraft in two or more sections. The margin against boom recontact was quantified based on the closest buckled hinge after the full length of the boom was reached and it was recoiling toward the spacecraft. An illustration showing the erosion of the recontact margin as the nearest buckled hinge moves closer to the spacecraft is presented in Fig. 13.

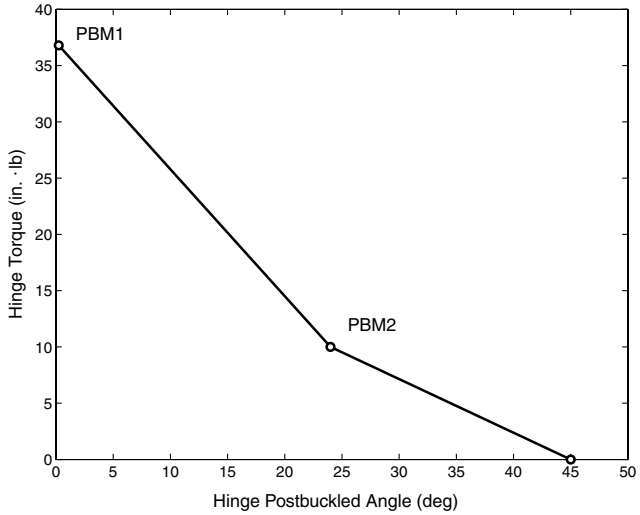

Fig. 12 Average hinge postbuckling deployment torque profile at −70 C used in the deployment simulation. PBM = postbuckling moment.

Results from the Monte Carlo study, shown in Fig. 14 and Table 3, indicated that there was a significant probability that the boom could contact the spacecraft or solar arrays during the deployment. The recontact cases tended to fall into one of three general categories: 1) a "slap" case (usually with a single buckled hinge), where the boom would have a sweeping motion so as to recontact with the side of the boom, 2) a "poke" or "fold" case (always with two or more buckled hinges), where the motion of the tip section of the boom was generally aligned with its long axis such that the tip would strike first, and 3) a "cradle" case which involved multiple buckled hinges and the risk that the boom could become entangled itself or on the spacecraft. To simplify the onerous task of assessing all 1000 cases a simple rule was applied that classified any penetration of the plane normal to the initial deployment as having a risk of contacting the spacecraft.

Figure 15 shows results from run 1 of the Monte Carlo and indicates the total boom kinetic energy, the cumulative number of hinge buckling events, and the point of closest approach for any beam node outboard of the buckled hinge closest to the spacecraft

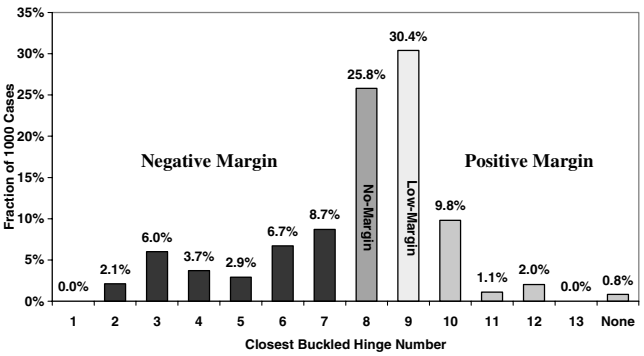

Fig. 14 Nominal Monte Carlo closest buckled hinge results at 2.5 s after boom release for all 1000 cases.

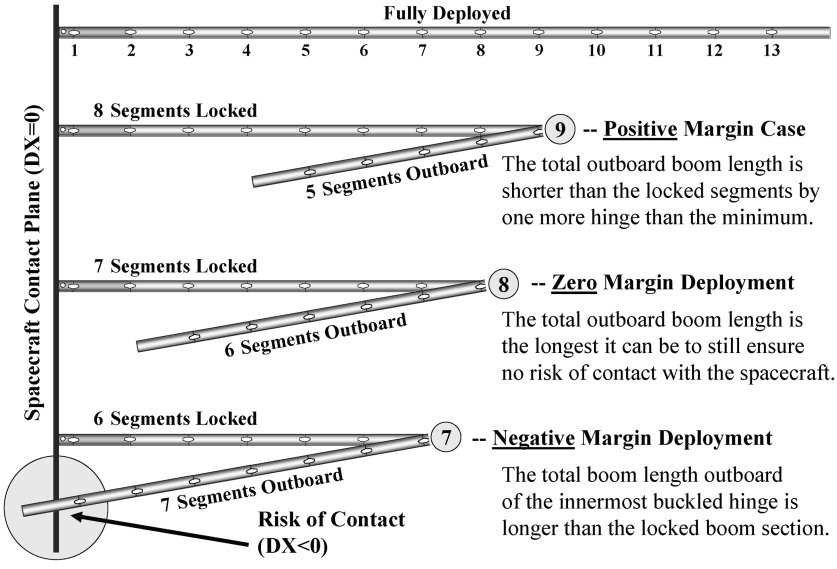

Fig. 13 The boom recontact margin is determined according to the buckled hinge closest to the spacecraft after the initial full extension of the boom (single buckled hinge case shown).

Table 3 Summary of Monte Carlo recontact types and probabilities

	Contact Cases	Slap Cases	Fold Cases	Cradle Cases
Boom 1	26%	15%	8%	3%
Boom 2	24%	13%	9%	2%

(not counting the root hinge). Note that the buckling events and the point of closest approach are plotted on the right-hand axis where the point of closest approach has been multiplied by a factor of 2 to make it more visible. Anytime the point of the closest approach line intersects the X axis then there is zero clearance to the $X = 0$ plane and the case is considered as presenting a risk of contact with the spacecraft. This metric is conservative as it does not include any 3-D motion which would considerably lower the contact probability. It is also interesting to note the sharp rise in buckling events that leads to a rapid decrease in kinetic energy at about 2.5 s. This is when the boom reaches its initial maximum extension and snaps through its nominal state due to the associated whipping action.

A failure modes analysis was done at ESA based on the energies and incidence angles obtained from the Monte Carlo runs. The conclusion of this analysis was that, although significant damage to the spacecraft was possible, the likelihood of it occurring was very low and the decision was made to proceed with the deployment.

III. Flight Deployment

Preparations for the flight deployment proceeded concurrently with the latter stages of the analysis and, once the risks had been vetted, the process necessary to deploy the antennas was engaged.

A. Deployment Dynamics Predictions

With no cameras available the onboard sensing of the MARSIS deployment was limited to 8 Hz sampling of the Mars Express rate gyros. All three of the MARSIS booms deploy primarily in the X–Z plane of Fig. 2 where the hinge axes of rotation are nominally aligned with the Y axis. Because the solar arrays are also deployed along the Y axis, the I_{yy} term is the minimum spacecraft inertia and is also the axis of principal interest as the largest rates were expected to be in the ω_y measurements. Rates about the X and Z axes are small and are dominated by the response of the solar arrays during the deployment. A compilation of ω_y results from the first 200 Monte Carlo runs is given in Fig. 16 for cases where the only remaining buckled hinge after the initial deployment was hinge 6 thru hinge 10.

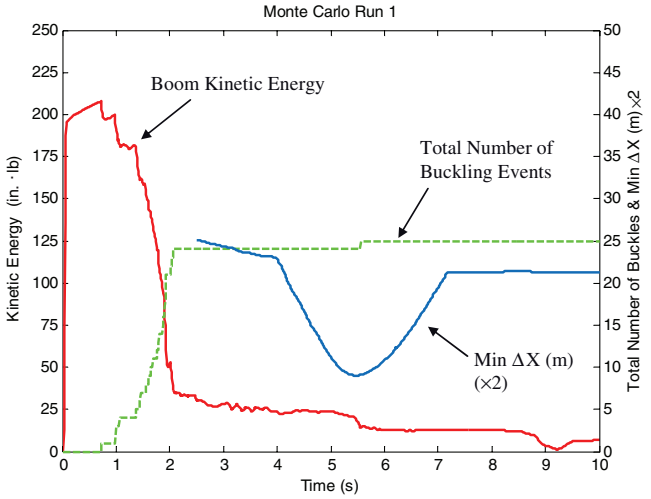

Fig. 15 Monte Carlo run 1 aggregate kinetic energy, hinge buckling, and outboard boom clearance results.

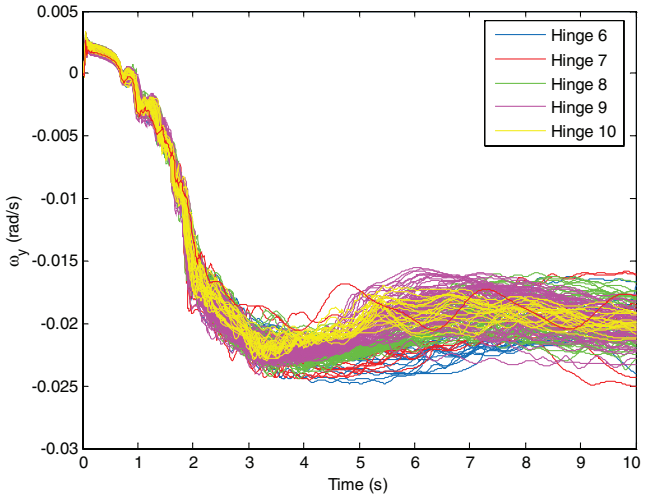

Fig. 16 Compilation of ω_y results for all single buckled hinge cases from the first 200 Monte Carlo cases.

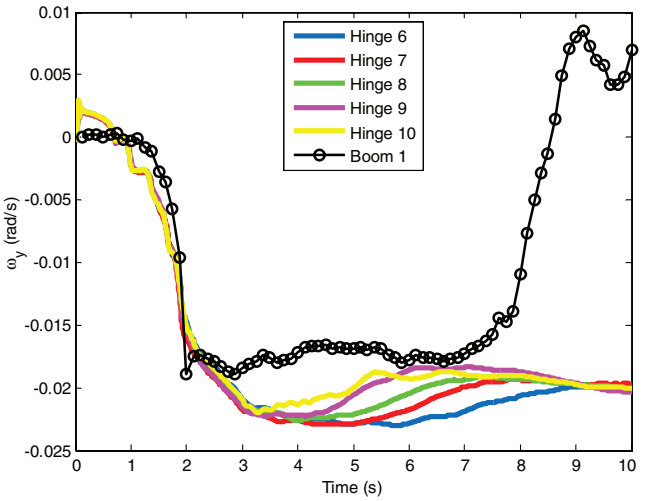

Fig. 17 Comparison of flight measured ω_y with average single buckled hinge Monte Carlo results from the first 200 cases.

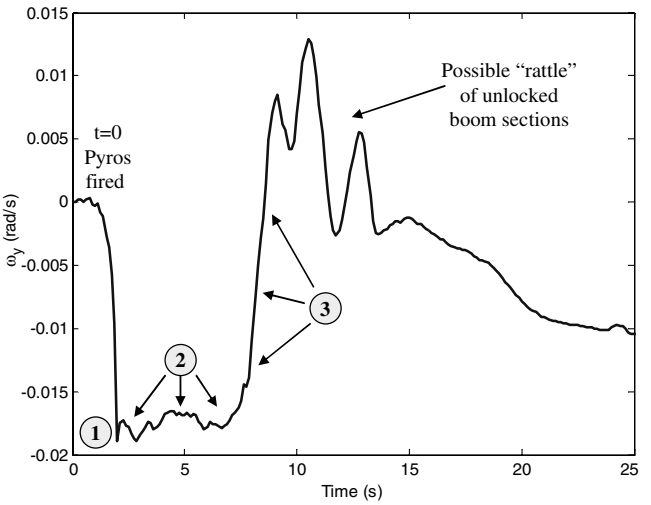

Fig. 18 Flight measured ω_y events: 1) initial snatch torque at ∼2 s; 2) nearly constant spacecraft rate over ∼2 to 7 s suggests that the boom may have multiple buckled hinges with the boom c.g. following a linear path; and 3) indications of possible locking of the root hinge at ∼7 s.

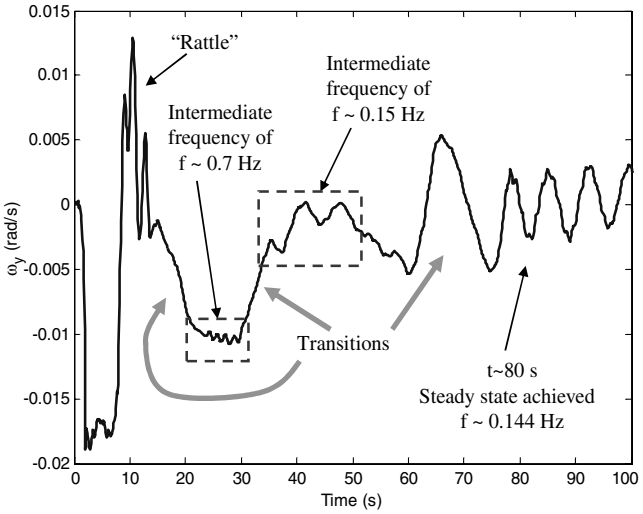

Fig. 19 During the subsequent time several intermediate frequencies are observed that likely indicate partially locked boom segments. There were at least four individual hinge locking or buckling events following the initial deployment phase (including hinge 10).

B. Flight Deployment Comparison

Dipole boom 1 was deployed on 4 May 2005, after which the spacecraft recovered from its postdeployment attitude and was stable. However, telemetry returned from the spacecraft indicated two anomalies in the deployment: first, the deployment dynamics were outside of the Monte Carlo simulations, and second, the spacecraft inertia and measured natural frequencies both indicated that the boom had not completely locked into place. The latter anomaly is not related to the deployment dynamics modeling and is discussed in a companion paper [6].

The 8 Hz flight data are compared to the average of the single buckled hinge cases in Fig. 17. A separate data set was also constructed that included all the multiple buckled hinge cases for comparison but a search of 1000 Monte Carlo cases did not find a good match. The ω_y rate matched reasonably well over the first 2 s and even the timing of the snatch load agreed quite well with the predicted behavior. However, there were two key features of the flight data in Fig. 17 that appear to have fallen outside of the Monte Carlo analysis: 1) the spacecraft angular rate maintains a nearly constant level over the period from 2 to 7 s, and 2) there is a sharp reversal of the spacecraft rate near 8 s that was not predicted in any of the original 1000 cases. Note that all of the Monte Carlo simulations were carried out for the first 10 s to see if the antenna

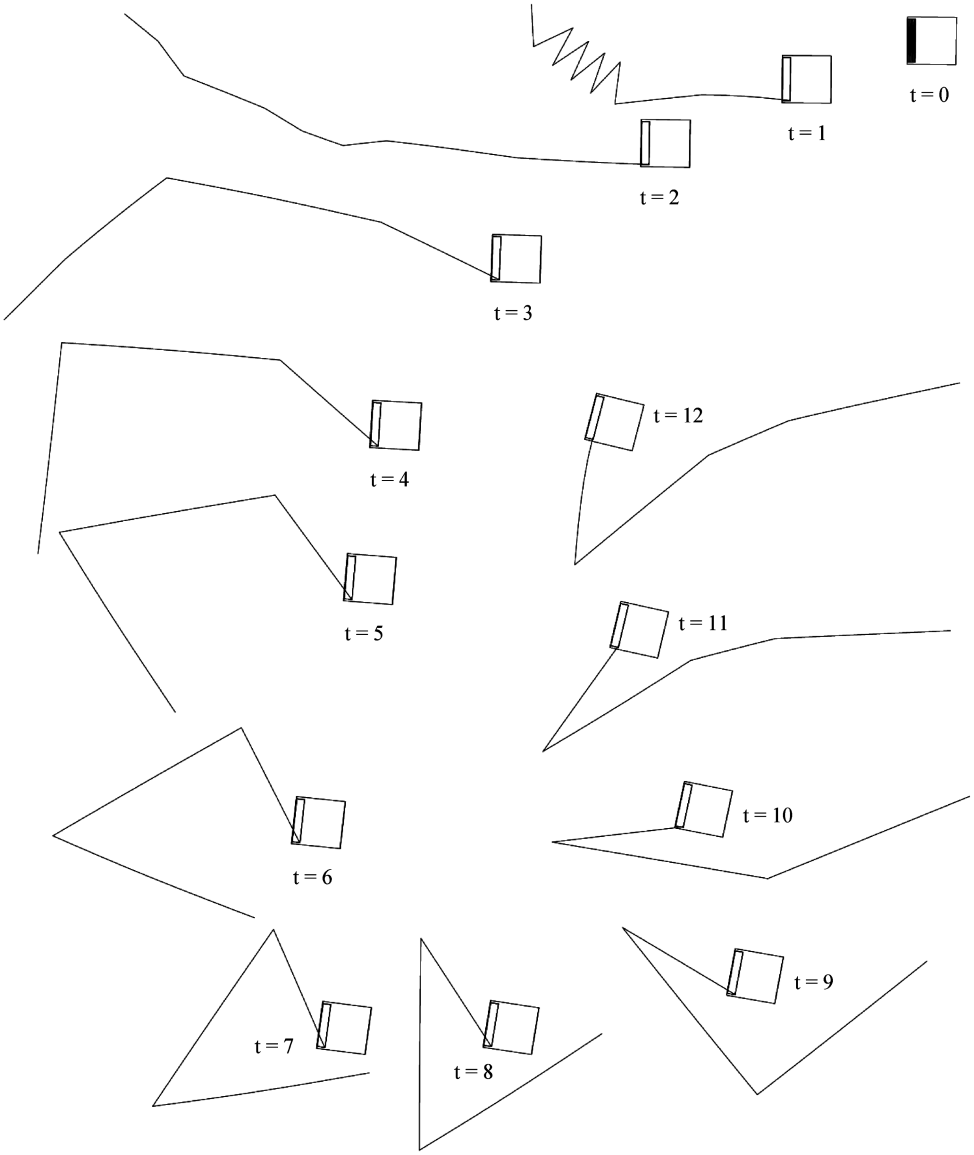

Fig. 20 Time sequence illustrating the boom geometries at 1 s intervals for the high hinges 1 and 2 increased strength run with $\zeta = 0.008$. Note that the locking of the root hinge causes a bending moment in the root segments at $t = 12$ s indicating a strong torque in the opposite direction of the initial boom snatch torque. This sharp reversal of torque was also observed in the boom-1 flight data.

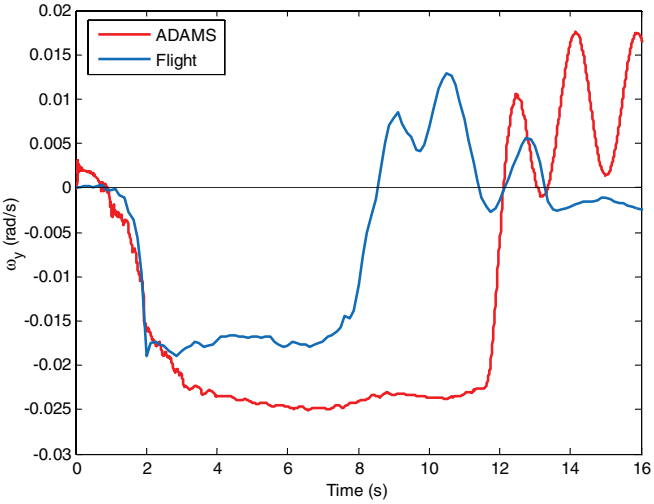

Fig. 21 Comparison of flight measured angular rates with the ADAMS results illustrated in Fig. 20. Note the key salient features common to both curves which include a rapid increase in rate near 2 s followed by a period of nearly constant angular rate and then a sharp reversal in the direction of rotation.

would impact the spacecraft which was the primary concern. The locking of the root hinge occurs after 10 s and was not observed in any of the Monte Carlo cases.

Further details of the complete flight deployment can be seen in the annotated Figs. 18 and 19 showing the spacecraft ω_y through the first 25 and 100 s, respectively. In particular, the second snatch loading is immediately followed by what appears to be a "rattling" of the boom which is likely accentuated by the lockout of the root hinge and a portion of the inboard boom resulting in a mechanical advantage for the loose outboard segments. These characteristics were duplicated in a separate ADAMS model that was modified in an attempt to reproduce this behavior. The ADAMS simulation is presented in Fig. 20 with a comparison of ω_y results to the flight data in Fig. 21. For this run the model was modified to include 0.8% modal damping and increased strength in hinges 1 and 2. Originally hinges 1 and 2 were assigned the same buckling strength as the outer hinges to conservatively assess the risk of spacecraft contact but they are actually significantly stronger. The 0.8% modal damping was determined from the flight data. The explanation for discrepancy between the ground test data (3.5%) and flight data is attributed mainly to the cold temperature. The ground test was performed at room temperature while the flight data were taken at an average temperature of −70°C. Test results indicated that the structural or hysteretic damping of the composite material was not temperature dependent. However, there are multiple bonded splices in the FFT that connect individual boom segments together. The adhesive used to bond the MARSIS tube assemblies was room temperature vulcanizing (RTV) silicone and it is a major contributor to the overall damping. Because the RTV glass transition temperature (T_g) is about −115°C, one could conclude that there would be a significant reduction in damping at cold temperatures.

Figure 19 shows several transitions as the boom slowly reaches varying degrees of deployment until, at approximately 80 s, steady-state dynamics are achieved. However, although the steady-state dynamics in Fig. 19 were initially encouraging, the most strongly excited frequency later measured from the flexible modes tests was found to be 0.146 Hz which was well above the predicted value of ∼0.1 Hz. In fact, there were initially three measured frequencies at 0.043 Hz, and 0.146 Hz about the Y axis and 0.076 Hz about the Z axis rather than the two expected frequencies at ∼0.1 Hz about the Y and Z axes. This indicated that dipole boom 1 did not achieve a full deployment and the resolution of this incomplete deployment which led to a successful deployment is discussed separately in the companion paper [6]. The main problem was that hinge 10 was not fully deployed (∼40 deg short) due to its on-orbit cold temperature (−140°C). Note that hinge characterization was done at −70°C and because the main concern was the high stowed energy the colder deployment was viewed as beneficial to reduce the deployment dynamics. Dipole boom 2 was later deployed successfully without any anomalies as was the monopole. The on-orbit telemetry is not adequate to detect the dynamics and consequently the full deployment of the ultralightweight monopole (0.31 lb) boom.

IV. Conclusions

First and foremost, the authors strongly recommend that the reader not take lenticular (carpenter tape) structures for granted. The mechanisms and sensitivities of these joints are complex and the use of multiple hinges greatly amplifies the modeling challenges. Material selection and construction can have subtle effects on the hinge behavior which, depending on the materials chosen, can also be strongly dependent on the in situ temperature. Ideally the hinges should have a positive torque margin throughout their range of motion. These hinge characteristics should be tested to verify their torque characteristics. The tests should closely approximate flight conditions especially temperature, aging, and thermal cycling effects, such as from aerobraking, whenever possible.

The total stowed energy should be optimized (neither too high nor too low) to control the dynamics in the deployment. The tube compression energy should be low enough to prevent the back-buckling phenomenon but, simultaneously, the hinge energy needs to be high enough to produce positive torque throughout the hinge range of motion. These types of lenticular booms are extremely lightweight and, once in their proper deployed state, are very easily modeled and accounted for on the spacecraft. Unfortunately, it is not possible to perform a meaningful full system test on the ground; hence, an accurate component model of the boom is extremely important.

Acknowledgments

The authors would like to acknowledge the hard work and thorough analysis of the European Space Agency's (ESA) and European Aeronautic Defence and Space Company (EADS) Astrium engineering and flight team as well as the important contributions of the analysis groups at Boeing Phantom Works for the DADS analysis and at ABAQUS West for the ABAQUS hinge analysis. In particular, the authors would like to thank Lou Adams and Olav Hallberg for their diligent work on the ADAMS simulation. The research described in this paper was carried out at NGST Astro Aerospace (Contract No. 1263269) and at the Jet Propulsion Laboratory, California Institute of Technology, under a contract with NASA.

References

[1] Marks, G. W., Reilly, M. T., and Huff, R. L., "The Lightweight Deployable Antenna for the MARSIS Experiment on the Mars Express Spacecraft," *Proceedings of the 36th Aerospace Mechanisms Symposium*, NASA CP-2002-211506, April 2002, pp. 183–196.

[2] Thomson, W. T., *The Theory of Vibration with Applications*, 2nd ed., Prentice–Hall, Upper Saddle River, NJ, 1981.

[3] Clough, R. W., and Penzien, J., *Dynamics of Structures*, McGraw–Hill, New York, 1975.

[4] Silver, M. J., Hinkle, J. D., and Peterson, L. D., "Modeling of Snap-Back Bending Response of Doubly Slit Cylindrical Shells," AIAA Paper 2004-1820, April 2004.

[5] Seffen, K. A., and Pellegrino, S., "Deployment Dynamics of Tape Springs," *Proceedings of the Royal Society of London A*, Vol. 455, No. 1983, March 1999, pp. 1003–1048.

[6] Adams, D. S., and Mobrem, M., "MARSIS Antenna Flight Deployment Anomaly and Resolution," AIAA Paper 2006-1684, May 2006.

L. Peterson
Associate Editor